

# Linear and nonlinear spin current response of anisotropic spin-orbit coupled systems

D. Muñoz-Santana<sup>1</sup> and Jesús A. Maytorena<sup>2</sup>

<sup>1</sup>*Centro de Investigación Científica y de Educación Superior de Ensenada, Baja California, Apartado Postal 360, 22860, Ensenada, Baja California, México.*

<sup>2</sup>*Centro de Nanociencias y Nanotecnología, Universidad Nacional Autónoma de México, Apartado Postal 14, 22800, Ensenada, Baja California, México.*

(Dated: March 1, 2023)

We calculate the linear and the second harmonic (SH) spin current response of two anisotropic systems with spin orbit (SO) interaction. The first system is a two-dimensional (2D) electron gas in the presence of Rashba and  $k$ -linear Dresselhaus SO couplings. The dependence of the anisotropic spin splitting on the sample growth direction introduces an additional path to modify the linear and nonlinear spectra. In particular, vanishing linear and second order spin conductivity tensors are achievable under SU(2) symmetry conditions, characterized by a collinear SO vector field. Additional conditions under which specific tensor components vanish are possible, without having such collinearity. Thus, a proper choice of the growth direction and SO strengths allows to select the polarization of the linear and SH spin currents according to the direction of flowing. The second system is an anisotropic 2D free electron gas with anisotropic Rashba interaction, which has been employed to study the optical conductivity of 2D puckered structures with anisotropic energy bands. The presence of mass anisotropy and an energy gap open several distinct scenarios for the allowed optical interband transitions, which manifest in the linear and SH response contrastingly. The linear response displays only out-of-plane spin polarized currents, while the SH spin currents flow with spin orientation lying parallel to the plane of the system strictly. The models illustrate the possibility of the nonlinear spin Hall effect in systems with SO interaction, under the presence or absence of time-reversal symmetry. The results suggest different ways to manipulate the linear and nonlinear optical generation of spin currents which could find spintronic applications.

## I. INTRODUCTION

The two-dimensional electron gas (2DEG) in semiconductor heterostructures has maintained its relevance even after almost two decades of constant discovery of new 2D materials. Even before graphene [1], these quantum wells were the subject of constant research due to their potential applications in the field of spintronics that the presence of spin-orbit (SO) coupling provides [2, 3]. The spin Hall effect [4], the current-induced spin polarization [5], a nonballistic version of a spin transistor [6, 7], and the persistent spin helix state [8] are remarkable examples of spin-dependent phenomena associated to the SO interaction in 2DEGs. The art of manipulating spin using SO coupling gave birth to the field called spin-orbitronics, also dubbed “Rashba-like physics” [9–11], inspired by the Rashba SO coupling, which leads to spin-momentum locking in low dimensional systems lacking inversion symmetry [3].

One of the most studied 2DEG systems is the one that includes the Rashba and the linear Dresselhaus SO contributions. The interplay between these couplings leads to an anisotropic spin-splitting responsible of effects like a characteristic frequency dependence of the charge and spin Hall conductivities [12], the anisotropy of plasmon dynamics [13], or persistent spin textures [14–16], among others. It also allows the possibility of spin-preserving symmetries and associated effects like the infinite spin lifetime due to fixed spin precession axis [15], the mentioned nonballistic spin-FET [6], the suppression of spin beats in oscillations of magnetoresistivity [17], the vanishing of *Zitterbewegung* [18, 19], the vanishing of the interband absorption and spin Hall conductivity [20], or the cancellation of plasmon damping [13], all with potential device applications. Despite the extensive research, the investigation has usually been restricted to quantum wells grown along the [001], [110], or [111] direction [6, 14, 15, 21–34]. It is until recently that attention has been paid to a general crystal orientation [35–37]. It was found that the recovery of the SU(2) symmetry can be realized for some growth direction Miller indices, with consequences like the transition from weak anti-localization to weak localization [35] or lifetime enhancement of spin helices [38]. Recently, the optical generation of dc spin currents by second-order nonlinear interactions in 2DEGs with SO coupling has also been explored [30, 39].

Another variant of 2D electron systems are new materials presenting a behavior similar to an electron gas with another type of in-plane anisotropy. These systems, such as phosphorene and group IV metal monochalcogenides, have an orthorhombic lattice and puckered structure with highly anisotropic energy bands, providing novel physical phenomena. Recently, the optical conductivity of such materials was calculated from a model Hamiltonian consisting of an anisotropic 2DEG [40] with an anisotropic Rashba splitting [41]. The optical absorption spectrum revealed a sensitive dependence on the mass anisotropy ratio and on the frequency and direction of the exciting field [42].

In this paper, we calculate the linear and the second harmonic (SH) spin current response of two anisotropic systems with SO interaction. First, we consider a 2DEG with Rashba and linear-in-momentum Dresselhaus couplings. We

explore how the dependence of the anisotropic spin splitting on the sample growth direction introduces an additional path to modify the linear and nonlinear spectra. In particular, we find that under SU(2) symmetry conditions, the linear and second order spin currents vanish. On the other hand, a proper choice of the growth direction and SO strengths allows to select their respective spin polarization according to the direction of flowing.

In reference [30], a nonlinear dc spin current generation of a Rashba-Dresselhaus coupled 2DEG, grown along the [001] direction, was investigated as an optical rectification response using a semiclassical Boltzmann approach in the relaxation-time approximation. Here instead, we focus on the finite frequency SH response in the clean limit of the system, and for arbitrary crystallographic direction of growth.

The second system is the same mentioned above [42] to study the optical response of 2D SO coupled puckered structures with mass anisotropy. We extend it by introducing an small energy gap in the Hamiltonian to represent a possible splitting of the conduction band [43]. This allows us to switch between a model which preserves the time-reversal symmetry (TRS) and one which breaks it. We find that the dependence of the spectrum of allowed interband transitions on the mass ratio and energy gap, leads to out-of-plane spin polarized linear currents, while the SH spin currents flow with the spin oriented parallel to the plane of the system strictly. Our results suggest different ways to manipulate the polarization and direction of the optically induced linear and SH spin current responses.

The paper is organized as follows. In section II the Kubo expressions for the dynamical linear and second-order spin current conductivity tensors of a generic two-band model are presented. In sections III we evaluate the formulae obtained in section II for the 2DEG with generic linear-in-momentum SO interaction and discuss the spectral features of the optical spin current response at the fundamental and SH frequencies. To this end, we first calculate the joint density of states (JDOS) and explain the origin of its van Hove singularities. Similarly, in section IV we discuss the spectral characteristics of the JDOS, and calculate the linear and SH spin current conductivities for the gapped anisotropic Rashba model. The conclusions are summarized in section V.

## II. FIRST AND SECOND ORDER KUBO FORMULAE

In this section we obtain the conductivity tensors characterizing the spin current response which depend linearly and quadratically on an externally applied electric field. We shall consider a generic two band model in 2D described by the momentum-space Hamiltonian  $H(\mathbf{k}) = \varepsilon_0(\mathbf{k})\mathbb{I} + \boldsymbol{\sigma} \cdot \mathbf{d}(\mathbf{k})$ , with energy spectrum  $\varepsilon_\lambda(\mathbf{k}) = \varepsilon_0(\mathbf{k}) + \lambda d(\mathbf{k})$ , where  $\mathbf{k}$  is the in-plane electron wave vector  $\mathbf{k} = k_x \hat{\mathbf{x}} + k_y \hat{\mathbf{y}} = k(\cos \theta \hat{\mathbf{x}} + \sin \theta \hat{\mathbf{y}})$ ,  $\mathbf{d}(\mathbf{k}) = d_x(\mathbf{k})\hat{\mathbf{x}} + d_y(\mathbf{k})\hat{\mathbf{y}} + d_z(\mathbf{k})\hat{\mathbf{z}}$ ,  $d(\mathbf{k}) = |\mathbf{d}(\mathbf{k})|$ ,  $\boldsymbol{\sigma}$  is the vector of Pauli matrices defined in the spin space,  $\mathbb{I}$  is the  $2 \times 2$  unit matrix, and  $\lambda = \pm$  specifies the helicity of the states in the upper (+) and lower (-) part of the spectrum. The eigenstates are  $|\lambda, \mathbf{k}\rangle = [N_\lambda, \lambda N_{-\lambda} \exp(i\phi)]^T$ , with  $[N_\lambda(\mathbf{k})]^2 = (d + \lambda d_z)/2d$  and  $\tan \phi(\mathbf{k}) = d_y/d_x$ . In what follows we simplify the notation and write  $|\lambda\rangle$  for this states.

Within the Kubo formalism, the linearly induced spin current is given by

$$\langle \mathcal{J}_i^\ell(t) \rangle^{(1)} = \frac{1}{i\hbar} \int_{-\infty}^t dt' \sum_{\lambda, \mathbf{k}} f(\varepsilon_\lambda(\mathbf{k})) \langle \lambda | [\hat{\mathcal{J}}_i^\ell(t), \hat{H}'(t')] | \lambda \rangle, \quad (1)$$

where all operators are in the interaction picture with respect to the unperturbed Hamiltonian. Here,  $\hat{\mathcal{J}}_i^\ell = \frac{\hbar}{4}(\sigma_\ell \hat{v}_i + \hat{v}_i \sigma_\ell)$  is the operator for the  $\ell$ -polarized spin current flowing in the  $i$ -direction, with  $\hbar \hat{v}_i = \partial H / \partial k_i$  defining the velocity operator component  $\hat{v}_i$ , ( $i = x, y; \ell = x, y, z$ ). The operator  $\hat{H}'(t) = (e/c)\hat{v}_i A_i(t)$  (sum over repeated index is assumed hereafter) contains the interaction of the electrons with a spatially homogeneous vector potential  $\mathbf{A}(t)$ , ( $e > 0$ ). The factor  $f_\lambda = f(\varepsilon_\lambda(\mathbf{k}))$  is the Fermi-Dirac occupation number of the band  $\varepsilon_\lambda(\mathbf{k})$ .

Assuming an applied uniform electric field of the form  $E_i(t) = E_i(\omega)e^{-i\omega t} + c.c. = -(1/c)\partial A_i / \partial t$ , the time integral leads to a first order induced spin current  $\langle \mathcal{J}_i^\ell(t) \rangle = e^{-i\omega t} \sigma_{ij}^\ell(\omega) E_j(\omega) + c.c.$ , with the spin conductivity tensor given by

$$\sigma_{ij}^\ell(\omega) = \frac{ie}{\hbar\tilde{\omega}} \sum_{\lambda\lambda'} \sum_{\mathbf{k}} (f_{\lambda'} - f_\lambda) \frac{\langle \lambda | \hat{\mathcal{J}}_i^\ell | \lambda' \rangle \langle \lambda' | \hat{v}_j | \lambda \rangle}{\tilde{\omega} - \omega_{\lambda'\lambda}}, \quad (2)$$

where  $\tilde{\omega} = \omega + i0^+$ ,  $i, j = x, y$  and  $\ell = x, y, z$ . Explicitly, we have

$$\sigma_{ij}^\ell(\omega) = \frac{ie}{2\hbar\omega} \int \frac{d^2k}{(2\pi)^2} (f_- - f_+) \frac{\partial \varepsilon_0}{\partial k_i} \frac{\partial d_p}{\partial k_j} \left\{ \frac{M_{\ell p}^+}{\hbar\tilde{\omega} + 2d} - \frac{M_{p\ell}^+}{\hbar\tilde{\omega} - 2d} \right\}, \quad (3)$$

where  $M_{ij}^\lambda(\mathbf{k}) = \langle \lambda | \sigma_i | -\lambda \rangle \langle -\lambda | \sigma_j | \lambda \rangle = (d^2 \delta_{ij} - d_i d_j) / d^2 + i \lambda \epsilon_{ijk} d_k / d$ .

At second order, the Kubo formula for the induced spin current reads as

$$\langle \mathcal{J}_i^\ell(t) \rangle^{(2)} = \frac{1}{(i\hbar)^2} \int_{-\infty}^t dt' \int_{-\infty}^{t'} dt'' \sum_{\lambda, \mathbf{k}} f(\varepsilon_\lambda(\mathbf{k})) \langle \lambda | [ [\hat{\mathcal{J}}_i^\ell(t), \hat{H}'(t')], \hat{H}'(t'') ] | \lambda \rangle. \quad (4)$$

For this case we assume an applied electric field  $E_i(t) = E_i(\omega_1)e^{-i\omega_1 t} + E_i(\omega_2)e^{-i\omega_2 t} + c.c.$  and focus on the sum frequency (SF) contribution proportional to  $E_j(t')E_l(t'')$ . The time integrals leads to a second order SF spin current  $\langle \mathcal{J}_i^\ell(t) \rangle_{SF} = e^{-i(\omega_1 + \omega_2)t} \sigma_{ijl}^{\ell, SF}(\omega_1, \omega_2) E_j(\omega_1) E_l(\omega_2) + c.c.$ , with the SF spin conductivity tensor given by

$$\sigma_{ijl}^{\ell, SF}(\omega_1, \omega_2) = \frac{e^2}{\hbar^2 \tilde{\omega}_1 \tilde{\omega}_2} \sum_{\wp} \sum_{\lambda \lambda' \lambda''} \int \frac{d^2 k}{(2\pi)^2} \frac{\langle \lambda | \hat{\mathcal{J}}_i^\ell | \lambda' \rangle \langle \lambda' | \hat{v}_j | \lambda'' \rangle \langle \lambda'' | \hat{v}_l | \lambda \rangle}{\tilde{\omega}_3 - \omega_{\lambda' \lambda}} \left( \frac{f_{\lambda''} - f_\lambda}{\tilde{\omega}_2 - \omega_{\lambda'' \lambda}} - \frac{f_{\lambda'} - f_{\lambda''}}{\tilde{\omega}_1 - \omega_{\lambda' \lambda''}} \right), \quad (5)$$

where  $i, j, l = x, y$  and  $\ell = x, y, z$ . Here  $\tilde{\omega}_i = \omega_i + i0^+$ ,  $i = 1, 2, 3$ ,  $\omega_3 = \omega_1 + \omega_2$ , and  $\sum_{\wp}$  stands for the intrinsic permutation symmetry  $(j, \omega_1) \leftrightarrow (l, \omega_2)$ . We shall be focused on the second harmonic response,  $\sigma_{ijl}^{\ell, (2\omega)}(\omega) = \sigma_{ijl}^{\ell, SF}(\omega, \omega)$ ,

$$\sigma_{ijl}^{\ell, (2\omega)}(\omega) = \frac{e^2}{(\hbar\tilde{\omega})^2} \sum_{\wp} \int \frac{d^2 k}{(2\pi)^2} (f_- - f_+) \frac{1}{d} \frac{\partial \varepsilon_0}{\partial k_i} \frac{\partial d_p}{\partial k_j} \frac{\partial d_q}{\partial k_l} \left[ \frac{d_l M_{pq}^+}{(\hbar\tilde{\omega})^2 - (2d)^2} - \frac{d_p M_{lq}^+}{(\hbar\tilde{\omega} + 2d)(2\hbar\tilde{\omega} + 2d)} - \frac{d_p M_{ql}^+}{(\hbar\tilde{\omega} - 2d)(2\hbar\tilde{\omega} - 2d)} \right]. \quad (6)$$

In the following, we use expressions (3) and (6) to study the spin current response of two anisotropic SO coupled systems.

### III. 2DEG WITH RASHBA AND DRESSELHAUS[ $hkl$ ] SO COUPLING

#### A. Joint density of states

We consider a 2DEG with an arbitrary crystal orientation defined by the unit normal  $\hat{\mathbf{n}} = n_x \hat{\mathbf{x}} + n_y \hat{\mathbf{y}} + n_z \hat{\mathbf{z}}$ , with underlying basis vectors  $\hat{\mathbf{x}}, \hat{\mathbf{y}}, \hat{\mathbf{z}}$ , pointing along the crystal axes [100], [010], [001], respectively. The system is in the presence of Rashba and linear-in- $k$  Dresselhaus SO couplings. The corresponding Hamiltonian is determined by the function  $\varepsilon_0(k_x, k_y) = \hbar^2 k^2 / 2m$  and the SO vector field  $d_i(k_x, k_y) = \mu_{i\nu} k_\nu$  ( $i = x, y, z; \nu = x, y$ ). For a given normal  $\hat{\mathbf{n}}$ , the  $xyz$  coordinate system can be rotated in order to obtain a new  $x'y'z'$  coordinate system, with the  $z'$ -axis pointing along the direction of  $\hat{\mathbf{n}}$ , and orthonormal basis  $\hat{\mathbf{l}}, \hat{\mathbf{m}}, \hat{\mathbf{n}}$ ,  $\hat{\mathbf{l}} = \hat{\mathbf{m}} \times \hat{\mathbf{n}}$ . Thus, for each orientation the matrix of SO material parameters  $\mu_{ij}$  must be understood as referred to the new coordinates, as well as the condition  $\mathbf{k} \cdot \hat{\mathbf{n}} = 0$ , which is transformed to the condition  $k'_z = 0$ . We shall use the symbol R+D[ $hkl$ ] to indicate the Rashba (R) and Dresselhaus (D) SO couplings when the sample is grown along the crystallographic direction [ $hkl$ ].

The  $k$ -space available for vertical transitions is determined by the condition  $\varepsilon_-(\mathbf{k}) \leq \varepsilon_F \leq \varepsilon_+(\mathbf{k})$  ('Pauli blocking'), and the conservation of energy  $\varepsilon_+(k_x, k_y) - \varepsilon_-(k_x, k_y) = \hbar\omega$ , for a given Fermi energy  $\varepsilon_F$  and exciting frequency  $\omega$ . This means that only those points  $(k_x, k_y)$  lying on the resonance curve  $C_r(\omega) = \{(k_x, k_y) | 2d(k_x, k_y) = \hbar\omega\}$  which satisfy the inequality  $k_F^+(\theta) < k < k_F^-(\theta)$  will contribute to the joint density of states (JDOS) [see Fig. 1(a)]. Here  $k_F^\lambda(\theta)$  are the Fermi contours, defined by the equation  $\varepsilon_\lambda(k_x, k_y) = \varepsilon_F$  which, written in polar coordinates, are given by  $k_F^\lambda(\theta) = \sqrt{2m\varepsilon_F/\hbar^2 + k_{so}^2(\theta)} - \lambda k_{so}(\theta)$ , where  $k_{so}(\theta) = mg_{[hkl]}(\theta)/\hbar^2$  is a characteristic wave number of the SO interaction. The function  $g_{[hkl]}(\theta)$  accounts for the anisotropy of the energy splitting  $2d(k_x, k_y) = 2kg_{[hkl]}(\theta)$ , with  $g_{[hkl]}(\theta) = |\boldsymbol{\mu}_x \cos \theta + \boldsymbol{\mu}_y \sin \theta|$ , where the vectors  $\boldsymbol{\mu}_\nu$ , with components  $(\boldsymbol{\mu}_\nu)_i = \mu_{i\nu}$ , are the columns of the matrix  $\mu_{i\nu}$ . The above restrictions imply that the allowed transitions are possible only in the energy window  $\hbar\omega_+(\theta) \leq \hbar\omega \leq \hbar\omega_-(\theta)$ , where  $\hbar\omega_\lambda(\theta) = 2d(k_F^\lambda(\theta)) = 2k_F^\lambda(\theta)g_{[hkl]}(\theta)$  is the minimum (maximum) photon energy  $\hbar\omega_+(\theta)$  ( $\hbar\omega_-(\theta)$ ) required to induce a vertical transition between states lying along the direction  $\theta$  in the  $k$ -space [inset in Fig. 1(a)]. As a consequence, the JDOS for the system with SOI R+D[ $hkl$ ] reads as

$$J_{+-}(\omega) = \frac{\hbar\omega}{16\pi^2} \int d\theta \frac{\Theta[1 - |\eta(\omega, \theta)|]}{g_{[hkl]}^2(\theta)}, \quad (7)$$

where  $\Theta(x)$  is the Heaviside unit step function, and  $\eta(\omega, \theta) = [\omega - \frac{1}{2}(\omega_-(\theta) + \omega_+(\theta))]/[\frac{1}{2}(\omega_-(\theta) - \omega_+(\theta))]$ . According to this expression the edges of the absorption spectrum will be at the photon energies  $\hbar\omega = \min_\theta \{\hbar\omega_+(\theta)\}$  and  $\hbar\omega = \max_\theta \{\hbar\omega_-(\theta)\}$ , which will occur along some directions  $\theta_<$  and  $\theta_>$  where the energy splitting is minimum and maximum, respectively. In general, the set of van Hove singularities can be identified geometrically by analyzing how

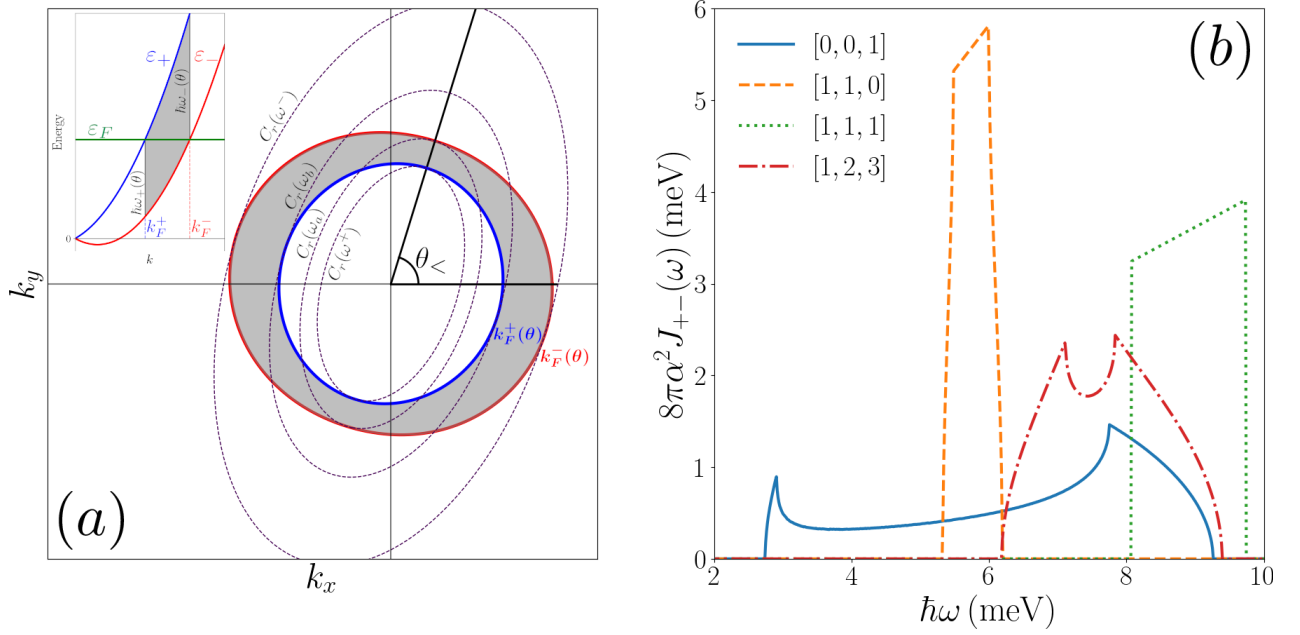


FIG. 1. (a) Fermi Contours  $k_F^\pm$  and resonance curves  $C_r(\omega)$  for the critical frequencies  $\omega^\pm, \omega_a, \omega_b$  ( $\omega^+ < \omega_a < \omega_b < \omega^-$ ) of a R+D[123] system. At temperature  $T = 0$ , the only states involved in vertical transitions between the bands  $\varepsilon_\lambda(\mathbf{k})$  (gray area) are those satisfying  $k_F^+(\theta) < k < k_F^-(\theta)$ , for which  $\varepsilon_-(\mathbf{k}) \leq \varepsilon_F \leq \varepsilon_+(\mathbf{k})$  (see inset). (b) The JDOS spectrum for several crystal orientations; the parameters used are  $\alpha = 160 \text{ meV \AA}$ ,  $\gamma k_n^2 = 0.5\alpha$ , and  $n = 5 \times 10^{11} \text{ cm}^{-2}$ ,  $m = 0.05m_0$  for the electron density and effective mass.

the resonance curve  $C_r(\omega)$  enters, intersects, and leaves the region of allowed transitions  $k_F^+(\theta) < k < k_F^-(\theta)$  [shaded area in Fig. 1(a)] as frequency varies. The resonance curve is a rotated ellipse with equation  $|k_x \mu_x + k_y \mu_y| = \hbar\omega/2$ . After a rotation by an angle  $\zeta$  defined by  $\tan 2\zeta = 2\mu_x \cdot \mu_y / (|\mu_x|^2 - |\mu_y|^2)$ , the ellipse becomes of the standard form with principal axes given by  $Q_x(\omega) = \hbar\omega/2g_{[hkl]}(\theta_<)$  and  $Q_y(\omega) = \hbar\omega/2g_{[hkl]}(\theta_>)$ , where  $\theta_> = \theta_< + \pi/2$ . In order to maintain the angle  $\theta_<$  as the direction of global minimum energy separation (as defined above) we choose  $\theta_< = \zeta$  if  $g_{[hkl]}(\zeta) < g_{[hkl]}(\zeta + \pi/2)$ , and  $\theta_< = \zeta + \pi/2$  otherwise. The critical van Hove energies are given by those values of  $\hbar\omega$  at which the axes  $Q_x(\omega)$  and  $Q_y(\omega)$  of the resonance ellipse touch tangentially the Fermi contours  $k_F^\pm(\theta)$  along  $\theta_<$  and  $\theta_>$ . Figure 1(a) illustrates the situation for the R+D[123] case. The critical frequencies are then defined by the matchings  $Q_x(\omega^+) = k_F^+(\theta_<)$ ,  $Q_x(\omega_a) = k_F^-(\theta_<)$ ,  $Q_y(\omega_b) = k_F^+(\theta_>)$ , and  $Q_y(\omega^-) = k_F^-(\theta_>)$ :

$$\hbar\omega^+ = 2k_F^+(\theta_<)g_{[hkl]}(\theta_<), \quad (8)$$

$$\hbar\omega_a = 2k_F^-(\theta_<)g_{[hkl]}(\theta_<), \quad (9)$$

$$\hbar\omega_b = 2k_F^+(\theta_>)g_{[hkl]}(\theta_>), \quad (10)$$

$$\hbar\omega^- = 2k_F^-(\theta_>)g_{[hkl]}(\theta_>). \quad (11)$$

Note that while  $\omega^+$  is always smaller than  $\omega^-$ , the order relation between  $\omega_a$  and  $\omega_b$  can change for different orientations.

In Fig. 1(b) we show the JDOS for different crystal orientations as a function of frequency, keeping the same SO parameters values. The overall shape and size of the spectra reveals a strong dependence on the direction of sample growth. For the case R+D[111], the Hamiltonian is formally identical to that of a system with Rashba coupling only, which presents an isotropic splitting of the states. Thus, the resonance curve and Fermi contours are concentric circles and the JDOS displays the well known box-like shape with only two spectral features ( $\hbar\omega^\pm$ ). However, for other orientations the  $k$ -space for allowed optical transitions becomes no longer isotropic, and two types of shapes may appear, depending on the relative values of  $\omega_a$  and  $\omega_b$ . When  $\omega_a < \omega_b$  the spectra can develop a convex shape between these critical energies, as shown in Fig. 1(b) for the R+D[001] and R+[123] systems. On the other hand, when  $\omega_a > \omega_b$  the JDOS presents a linear dependence instead, as is illustrated by the R+D[110] case. This can be explained by observing how the resonance curve  $C_r(\omega)$  overlaps the region of allowed transitions bounded by the Fermi contours in each case. When  $\omega_a < \omega_b$ , the semi-axis  $Q_x(\omega)$  of the curve  $C_r(\omega)$  will reach the line  $k_F^-(\theta)$  first before the semi-axis  $Q_y(\omega)$  intersects the line  $k_F^+(\theta)$ , which means that for  $\omega_a < \omega < \omega_b$  there is a portion of the curve

which does not contribute to the JDOS. In contrast, when  $\omega_a > \omega_b$  we have the opposite situation, the semi-axis  $Q_x(\omega)$  touch the Fermi contour  $k_F^-(\theta)$  after the axis  $Q_y(\omega)$  contacts the Fermi contour  $k_F^+(\theta)$ . This imply that there is a range of frequencies,  $\omega_b < \omega < \omega_a$ , for which the ellipses  $C_r(\omega)$  lie entirely within the allowed zone (shaded area in Fig. 1(a)), causing a linear increase in the JDOS. The dependence of the critical frequencies (8)-(11) on the Miller indices, suggests the growth direction as an additional element of control of the spectrum of optical transitions.

### B. First order spin current conductivity

The spin conductivity tensor at the fundamental frequency for the SO coupled 2DEG, as obtained from Kubo formula (3), is (no sum over repeated indices is implied)

$$\text{Re } \sigma_{ij}^\ell(\omega) = \sigma_{ij}^\ell(0) - \frac{e}{8\pi} (\boldsymbol{\mu}_x \times \boldsymbol{\mu}_y)_\ell \frac{\hbar\omega}{8m/\hbar^2} \frac{1}{2\pi} \int_0^{2\pi} \frac{d\theta}{g^4(\theta)} \ln \left| \frac{[\omega + \omega_+(\theta)][\omega - \omega_-(\theta)]}{[\omega - \omega_+(\theta)][\omega + \omega_-(\theta)]} \right| \times [\epsilon_{ijz} + \sin 2\theta (\delta_{iy} - \delta_{ix}) \delta_{ij} + \cos 2\theta (1 - \delta_{ij})] \quad (12)$$

$$\text{Im } \sigma_{ij}^\ell(\omega) = -\frac{e}{8\pi} (\boldsymbol{\mu}_x \times \boldsymbol{\mu}_y)_\ell \frac{\hbar\omega}{16m/\hbar^2} \int_0^{2\pi} \frac{d\theta}{g^4(\theta)} [\epsilon_{ijz} + \sin 2\theta (\delta_{iy} - \delta_{ix}) \delta_{ij} + \cos 2\theta (1 - \delta_{ij})] \Theta[1 - |\eta(\omega, \theta)|], \quad (13)$$

where

$$\sigma_{ij}^\ell(0) = -\frac{e}{8\pi} (\boldsymbol{\mu}_x \times \boldsymbol{\mu}_y)_\ell \frac{1}{2\pi} \int_0^{2\pi} \frac{d\theta}{g^2(\theta)} [\epsilon_{ijz} + \sin 2\theta (\delta_{iy} - \delta_{ix}) \delta_{ij} + \cos 2\theta (1 - \delta_{ij})], \quad (14)$$

is the dc spin conductivity. Note that  $\sigma_{yy}^\ell(\omega) = -\sigma_{xx}^\ell(\omega)$ . Complex integration gives the result

$$\sigma_{ij}^\ell(0) = -\frac{e}{8\pi} \frac{(\boldsymbol{\mu}_x \times \boldsymbol{\mu}_y)_\ell}{|\boldsymbol{\mu}_x \times \boldsymbol{\mu}_y|} \begin{pmatrix} -\text{Im}(z_+) & 1 + \text{Re}(z_+) \\ -1 + \text{Re}(z_+) & \text{Im}(z_+) \end{pmatrix}, \quad (15)$$

where

$$z_+ = -\frac{[A - \sqrt{A^2 - (B^2 + C^2)}]}{B^2 + C^2} (B + iC), \quad (16)$$

with  $A = (|\boldsymbol{\mu}_x|^2 + |\boldsymbol{\mu}_y|^2)/2$ ,  $B = (|\boldsymbol{\mu}_x|^2 - |\boldsymbol{\mu}_y|^2)/2$ , and  $C = \boldsymbol{\mu}_x \cdot \boldsymbol{\mu}_y$ . The general expression (15) extends the result reported in Ref. [44], which is valid for SO vector fields with  $d_z(\mathbf{k}) = 0$  ( $\mu_{zx} = \mu_{zy} = 0$ ) only.

Since  $(\boldsymbol{\mu}_x \times \boldsymbol{\mu}_y)_x$  and  $(\boldsymbol{\mu}_x \times \boldsymbol{\mu}_y)_y$  vanish for  $\mu_{zv} = 0$  we have that the only systems supporting a linear spin current with perpendicular-to-plane spin polarization strictly, are those grown along the [001] and [111] directions; any other crystal orientation will have in-plane spin polarized current components. Moreover, the vanishing of the common factor  $\boldsymbol{\mu}_x \times \boldsymbol{\mu}_y$  implies the absence of an induced spin current via electric-dipole interaction in the 2DEG with R+D[ $hkl$ ] SO coupling. This reminds the well known effects due to the recovery of the SU(2) symmetry predicted in systems with R+D[001], like the infinite spin lifetime due to fixed spin precession axis [15] or the formation of a persistent spin helix state [14, 16].

As we mentioned before, Kammermeier et al.[35] found that for an arbitrary crystal orientation is still possible to have conditions for spin-preserving symmetries due to the interplay of Rashba and Dresselhaus SOI. The requirement for that is to have samples with two Miller indices equal in modulus and a particular relation between the Rashba and Dresselhaus parameters (in our language, a proper combination of the elements of the SO matrix  $\mu_{ij}$ ) [35]. It can be verified that for these special conditions, the factor  $\boldsymbol{\mu}_x \times \boldsymbol{\mu}_y$  is zero. Without loss of generality, lets choose, after Kammermeier, the orientation  $\hat{\mathbf{n}} = (\eta, \eta, n_z)$ , with  $\hat{\mathbf{m}} = (-1, 1, 0)/\sqrt{2}$  and  $\hat{\mathbf{l}} = (n_z, n_z, -2\eta)/\sqrt{2}$ , where  $n_z^2 = (1 - 2\eta^2)$ . The corresponding vectors of SO parameters become  $\boldsymbol{\mu}_x = (0, -\alpha + \gamma k_n^2 (1 - 9\eta^2) n_z, 0)$  and  $\boldsymbol{\mu}_y = (\alpha + \gamma k_n^2 (1 + 3\eta^2) n_z, 0, -\gamma k_n^2 \sqrt{2} \eta (1 - 3\eta^2))$ , where  $\alpha$  and  $\gamma k_n^2$  are the Rashba and Dresselhaus coupling strengths, respectively. When these satisfy the relation  $\alpha/\gamma k_n^2 = (1 - 9\eta^2) n_z$  ( $\mu_{yx} = 0$ ), the SO vector field becomes collinear,  $\mathbf{d}(\mathbf{k}) = \gamma k_n^2 (3\eta^2 - 1) (-2n_z, 0, \sqrt{2} \eta) k_y$ . Under these conditions,  $\boldsymbol{\mu}_x \times \boldsymbol{\mu}_y = \mu_{yx} (\mu_{zy}, 0, -\mu_{xy}) = 0$ , implying the vanishing of the spin current. Note also that when  $\mu_{yx} \neq 0$ , and  $\mu_{zy} = 0$  (which is true for the [111] growth direction only,  $\eta^2 = 1/3$ ) or  $\mu_{xy} = 0$ , the polarization of the spin current is along the direction  $\hat{\mathbf{n}}$  ( $z'$ ) or  $\hat{\mathbf{l}}$  ( $x'$ ), respectively. In contrast, the spin current polarized parallel to the  $\hat{\mathbf{m}}$  direction is null regardless the magnitude of the SO strength parameters,  $\sigma_{ij}^y(\omega) = 0$ . Interestingly, although the condition  $\mu_{xy} = 0$ , which rewrites as  $\alpha/\gamma k_n^2 = -(1 + 3\eta^2) n_z$ , does not corresponds to a collinear SO vector field, still produces an absence of out-of-plane-polarized spin current.



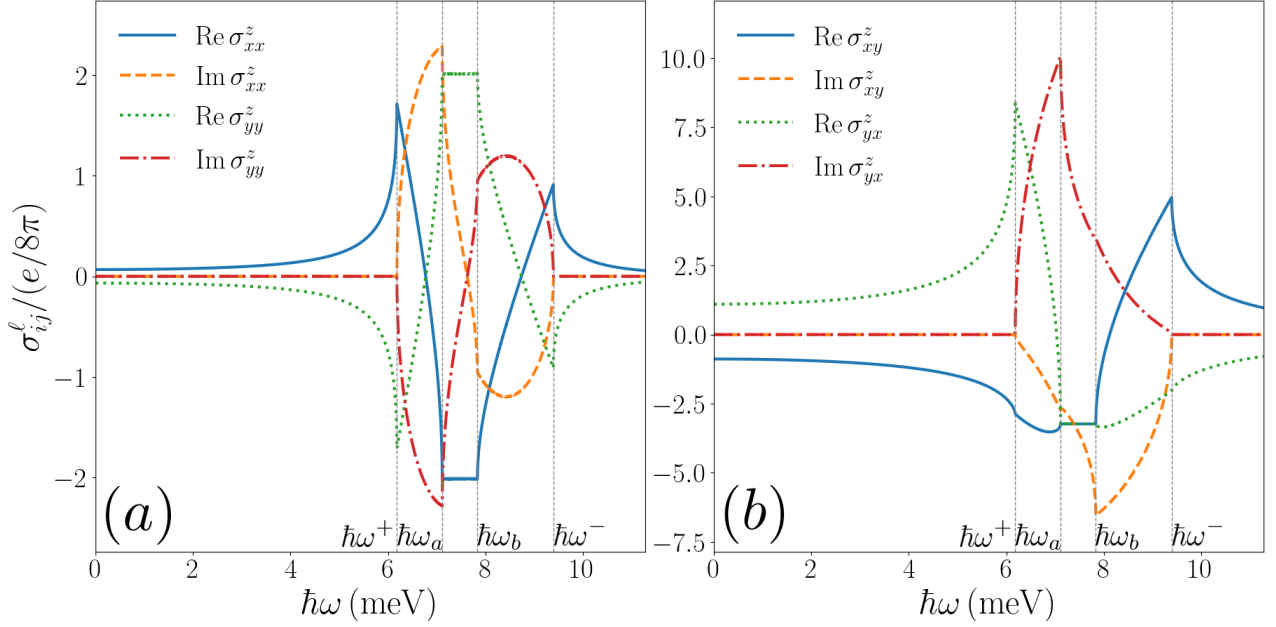


FIG. 2. Longitudinal (a) and transverse (b) components of the linear spin current conductivity  $\sigma_{ij}^z(\omega)$  for a R+D[123] 2DEG. The vertical dotted lines indicate the positions of the critical frequencies. The parameters used are the same as in Fig. 1.

In Fig. 2, a typical spectrum of the linear spin current conductivity  $\sigma_{ij}^z(\omega)$  is displayed, in this case for the R+D[123] system. As anticipated by the JDOS, we can identify the presence of van Hove features at the critical energies (8)-(11), defined by the Pauli blocking and the energy conservation condition for vertical transitions (Fig. 1(b)). Given that the critical frequencies (8)-(11) depend not only on the magnitude and relative value of the SO material parameters but also on the crystal orientation, our results suggests a kind of spectral control of the overall shape of the linear spin current response by choosing appropriately the samples in advance.

### C. SH spin current conductivity

The second-order Kubo formula (6) leads to the SH spin conductivity of the R+D[ $hkl$ ] system,

$$\sigma_{ijl}^{\ell,(2\omega)}(\omega) = \frac{e^2}{(\hbar\omega)^2} \frac{(\hbar^2/m)}{(2\pi)^2} (\boldsymbol{\mu}_x \times \boldsymbol{\mu}_y)_p \int_0^{2\pi} \frac{d\theta}{g^6(\theta)} \hat{k}_i \hat{k}_\nu \left\{ (\boldsymbol{\mu}_x \times \boldsymbol{\mu}_y)_p \mu_{\ell\nu} (\delta_{jl} - \hat{k}_j \hat{k}_l) C(\omega, \theta) \right. \\ \left. - \epsilon_{\ell pq} \mu_{qp} \hat{k}_\rho (\boldsymbol{\mu}_j \cdot \boldsymbol{\mu}_\nu) (\hat{k}_x \delta_{l\nu} - \hat{k}_y \delta_{lx}) [C(\omega, \theta) - 4C(2\omega, \theta)] + (j \leftrightarrow l) \right\} \quad (17)$$

where  $\hat{k}_i(\theta) = \cos\theta\delta_{ix} + \sin\theta\delta_{iy}$  and

$$C(x, \theta) = -\frac{1}{4} \left( \frac{2mg^2(\theta)}{\hbar^2} + \frac{\hbar x}{4} \ln \left| \frac{[x + \omega_+(\theta)][x - \omega_-(\theta)]}{[x - \omega_+(\theta)][x + \omega_-(\theta)]} \right| \right) - i\pi \frac{\hbar x}{16} \Theta[1 - |\eta(x, \theta)|]. \quad (18)$$

As in the linear response, the system grown along  $\hat{\mathbf{n}} = (\eta, \eta, n_z)$  will not support a spin current at  $2\omega$  when  $\mu_{yx} = 0$ , or equivalently when the SO field  $d_i(\mathbf{k}) = \mu_{i\nu} k_\nu$  becomes collinear. However, for the same special class of orientations, to analyze the spin conductivity for each spin index  $\ell$ , we have to focus in the following factors

$$(\boldsymbol{\mu}_x)_\ell = \mu_{yx} \delta_{\ell y}, \quad (19)$$

$$(\boldsymbol{\mu}_y)_\ell = (\mu_{xy} \delta_{\ell x} + \mu_{zy} \delta_{\ell z}), \quad (20)$$

$$[(\boldsymbol{\mu}_x \times \boldsymbol{\mu}_y) \times \boldsymbol{\mu}_x]_\ell = \mu_{yx}^2 (\mu_{xy} \delta_{\ell x} + \mu_{zy} \delta_{\ell z}), \quad (21)$$

$$[(\boldsymbol{\mu}_x \times \boldsymbol{\mu}_y) \times \boldsymbol{\mu}_y]_\ell = -\mu_{yx} (\mu_{xy}^2 + \mu_{zy}^2) \delta_{\ell y}. \quad (22)$$

We note that there are some possibilities to control the polarization of the nonlinear spin current. For  $\mu_{yx} \neq 0$ , the condition  $\mu_{xy} = 0$  ( $\mu_{zy} = 0$ ) corresponds to have a spin current flowing in the plane defined by  $\hat{\mathbf{m}}$  and  $\hat{\mathbf{n}}$  ( $\hat{\mathbf{1}}$  and

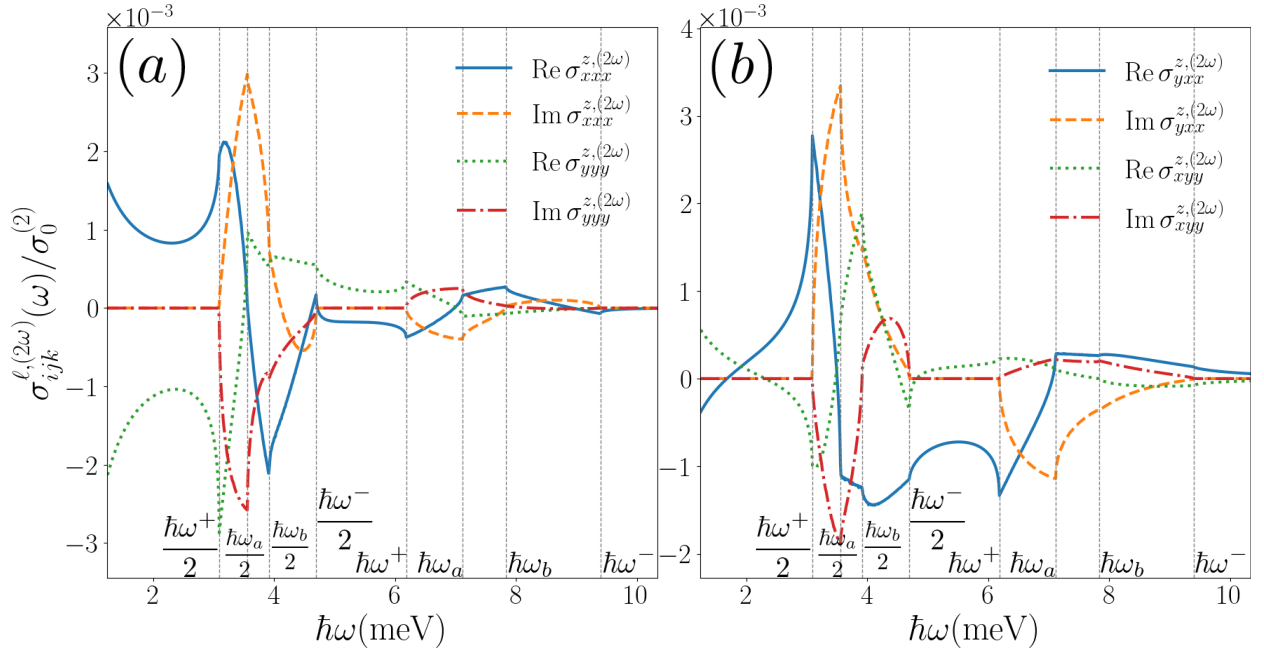


FIG. 3. Longitudinal (a) and Hall (b) components of the second-harmonic spin current conductivity tensor with out-of plane spin orientation for a R+D[123] 2DEG, where  $\sigma_0^{(2)} = e^2\alpha/4\pi\varepsilon_R^2$ ,  $\varepsilon_R = m\alpha^2/\hbar^2$ . The parameters used are the same as in Fig. 1.

$\hat{\mathbf{m}})$ , that is  $\sigma_{ijl}^{x,(2\omega)}(\omega) = 0$  ( $\sigma_{ijl}^{z,(2\omega)}(\omega) = 0$ ). On the other hand, to have  $\sigma_{ijl}^{y,(2\omega)}(\omega) = 0$  is possible only for  $\mu_{yx} = 0$ . Therefore, we have that for a system with crystal orientation  $\hat{\mathbf{n}} = (\eta, \eta, n_z)$ , and given that the linear  $\sigma_{ij}^y(\omega) = 0$ , the generation of a spin current polarized along the  $\hat{\mathbf{m}}$  ( $y'$ ) direction will depend quadratically on the electric field, because it is induced as a second-order response strictly.

Fig. 3 shows the SH spin current conductivity  $\sigma_{ijl}^{z,(2\omega)}(\omega)$  for the R+D[123] system. As expected, beside the peaks related with critical points at the energies  $\hbar\omega^\pm, \hbar\omega_a, \hbar\omega_b$ , van Hove singularities appear also at their subharmonics. Similarly to the first-order spin current conductivity, the magnitude and direction of the nonlinear spin current could be modified through frequency variation, relative value of the SO strengths, or by a proper choice of the sample growth direction.

Another aspect worth noting is that the R+D[ $hkl$ ] systems will present a nonlinear spin Hall effect, through  $\sigma_{yxx}^{z,(2\omega)}(\omega) \neq 0$  and  $\sigma_{xyy}^{z,(2\omega)}(\omega) \neq 0$ , except for R+D[001] and R+D[111] cases. The necessary condition for this phenomenon is to have  $d_z(\mathbf{k}) \neq 0$  ( $\mu_{z\nu} \neq 0$ ), which is characteristic of [110] samples, one of the low Miller indices usually studied.

## IV. 2D ANISOTROPIC RASHBA MODEL

### A. Energy spectrum and the joint density of states

In this section we considered another anisotropic model, used to study the effect of an anisotropic Rashba splitting on the longitudinal optical conductivity of 2D puckered structures [42] like black phosphorus and group IV monochalcogenides [45–47]. Here the reduced symmetry of the splitting of the states is due to mass anisotropy. The kinetic contribution to the low energy Hamiltonian is that of an anisotropic free electron gas [40, 48],  $\varepsilon_0(\mathbf{k}) = \hbar^2 k_x^2/2m_x + \hbar^2 k_y^2/2m_y$ , while the Rashba SO field is taken as  $\mathbf{d}(\mathbf{k}) = \alpha(\sqrt{m_d/m_y}k_y\hat{\mathbf{x}} - \sqrt{m_d/m_x}k_x\hat{\mathbf{y}}) + \Delta\hat{\mathbf{z}}$ , where  $\alpha$  is the SO strength and  $m_d = \sqrt{m_x m_y}$  is the geometric mean of the masses  $m_x$  and  $m_y$  along the  $x$ - and  $y$ - directions [41]. The model has been extended to include an energy parameter,  $\Delta \geq 0$ , which gives rise to a gap in the energy dispersion; by taking  $\Delta = 0$  or  $\Delta \neq 0$  we can move from a model with TRS to a model with broken TRS. This massive anisotropic Rashba low-energy model could describe a gapped conduction band of the phosphorene monolayer [43].

Written in polar coordinates, the conduction ( $\lambda = +$ ) and valence ( $\lambda = -$ ) bands are  $\varepsilon_\lambda(k, \theta) = \hbar^2 k^2 g^2(\theta)/2m_d + \lambda\sqrt{\alpha^2 k^2 g^2(\theta) + \Delta^2}$ . The function  $g(\theta) = [(m_d/m_x)\cos^2\theta + (m_d/m_y)\sin^2\theta]^{1/2}$  measures the separation of energy-constant curves along the direction  $\theta$  in the  $k$ -space; note that  $g(\theta) = 1$  when  $m_x = m_y$ , which corresponds to the well

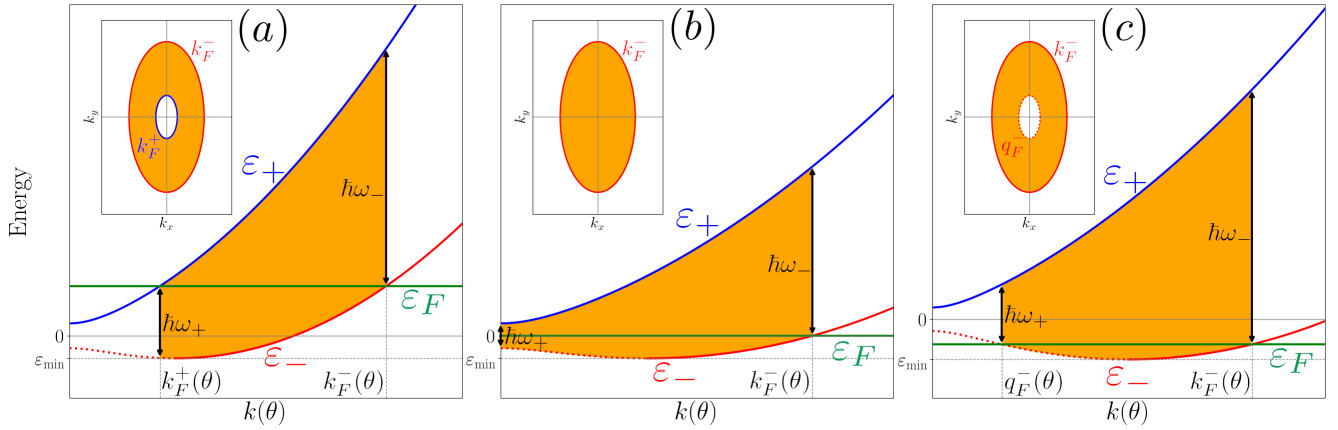


FIG. 4. Energy bands  $\varepsilon_{\pm}(k, \theta)$  of a gapped 2D anisotropic Rashba model when  $\varepsilon_R > \Delta$ . The shaded areas indicate the  $k$ -region of allowed optical transitions for several Fermi level positions: (a)  $\varepsilon_F > \Delta$ , (b)  $|\varepsilon_F| < \Delta$  and (c)  $\varepsilon_{min} < \varepsilon_F < -\Delta$ . The insets show the respective Fermi contours.

known case of a magnetized 2DEG with Rashba coupling in quantum wells of semiconductor heterostructures [49]. The energy difference between the bands is  $\varepsilon_+(\mathbf{k}) - \varepsilon_-(\mathbf{k}) = 2d(\mathbf{k}) = 2\sqrt{\alpha^2 k^2 g^2(\theta) + \Delta^2}$  and the constant energy-difference curve,  $C_r(\omega) = \{(k_x, k_y) | \varepsilon_+(\mathbf{k}) - \varepsilon_-(\mathbf{k}) = \hbar\omega\}$  is the ellipse with equation  $\varepsilon_0(k_x, k_y) = [(\hbar\omega/2)^2 - \Delta^2]/2\varepsilon_R$ , where  $\varepsilon_R = m_d \alpha^2 / \hbar^2$  is a characteristic energy associated to the Rashba interaction.

The shape of the band  $\varepsilon_-(\mathbf{k})$  depends on the ratio  $p = \Delta/\varepsilon_R$ . When  $p < 1$ , the band acquires a mexican hat shape, with a local maximum  $-\Delta$  at the origin  $\mathbf{k} = \mathbf{0}$  and two local minimums of value  $\varepsilon_{min} = -(\varepsilon_R^2 + \Delta^2)/2\varepsilon_R$  at  $\mathbf{k}$ -points lying on the ellipse  $\varepsilon_0(k_x, k_y) = (\varepsilon_R^2 - \Delta^2)/2\varepsilon_R$ . Otherwise, the valence band develops only a minimum at the origin. This means that there are several distinct positions for the Fermi level: (i)  $\varepsilon_F > \Delta$  (Fig. 4(a)), and then two Fermi contours are generated

$$k_F^{\pm}(\theta) = \frac{1}{\alpha g(\theta)} \left[ \left( \sqrt{\varepsilon_R^2 + \Delta^2 + 2\varepsilon_R \varepsilon_F \mp \varepsilon_R} \right)^2 - \Delta^2 \right]^{1/2}, \quad (23)$$

from equations  $\varepsilon_+(k, \theta) = \varepsilon_-(k, \theta) = \varepsilon_F$ ; (ii)  $|\varepsilon_F| < \Delta$  (Fig. 4(b)), where there is only one Fermi contour  $k_F^-(\theta)$ , lying on the valence band; and (iii) if  $p < 1$ ,  $\varepsilon_{min} < \varepsilon_F < -\Delta$  (Fig. 4(c)), where the Fermi lines arise only from the valence band through the equation  $\varepsilon_-(k, \theta) = \varepsilon_F$ , with roots  $k_F^-(\theta)$  and

$$q_F^-(\theta) = \frac{1}{\alpha g(\theta)} \left[ \left( \varepsilon_R - \sqrt{\varepsilon_R^2 + \Delta^2 + 2\varepsilon_R \varepsilon_F} \right)^2 - \Delta^2 \right]^{1/2}. \quad (24)$$

Note that the situation (i) or (iii) includes the gappless case  $\Delta = 0$ , the Fermi level being then positive or negative, respectively.

Interestingly, the Fermi lines described by (23) and (24) are concentric ellipses vertically (horizontally) oriented if  $m_y > m_x$  ( $m_x > m_y$ ), see insets in Fig. 4. The energy separation of the bands at these lines is independent of the direction  $\theta$  in  $k$ -space, taking the values  $2d(k_F^{\pm}(\theta)) = 2\left(\sqrt{\varepsilon_R^2 + \Delta^2 + 2\varepsilon_R \varepsilon_F \mp \varepsilon_R}\right)$  or  $2d(q_F^-(\theta)) = 2\left(\varepsilon_R - \sqrt{\varepsilon_R^2 + \Delta^2 + 2\varepsilon_R \varepsilon_F}\right)$ , according to the position of the Fermi level.

The lowest (highest) energy of the spectrum of allowed interband transition will be denoted by  $\hbar\omega_+$  ( $\hbar\omega_-$ ), see Fig. 4. When  $|\varepsilon_F| < \Delta$  we have that the lowest possible transition occurs at the energy gap  $\hbar\omega_+ = 2\Delta$ . When  $\varepsilon_F > \Delta$  or  $\varepsilon_{min} < \varepsilon_F < -\Delta$ , we have  $\hbar\omega_+ = 2d(k_F^{\pm})$  or  $\hbar\omega_+ = 2d(q_F^-)$ , respectively. The highest possible energy transition is always given by  $\hbar\omega_- = 2d(k_F^-)$ . Moreover, the resonance curve  $C_r(\omega)$  is an ellipse with the same shape and orientation than the Fermi lines, but differing only in size given its frequency dependence. As a consequence, there will be only two critical points in the JDOS, given by the frequencies  $\omega_+$  and  $\omega_-$  at which the ellipse  $C_r(\omega)$  enters and leaves, respectively, the region of allowed transitions (shaded areas in the insets of Fig. 4), and which defines an absorption window  $\hbar\omega_+(\varepsilon_F) < \hbar\omega < \hbar\omega_-(\varepsilon_F)$ . All this is apparent in the JDOS

$$J_{+-}(\omega; \varepsilon_F) = \frac{\hbar\omega}{8\pi\alpha^2} \Theta(1 - |\eta(\omega, \varepsilon_F)|), \quad \eta(\omega, \varepsilon_F) = \frac{\omega - (\omega_- + \omega_+)/2}{(\omega_- - \omega_+)/2}, \quad (25)$$



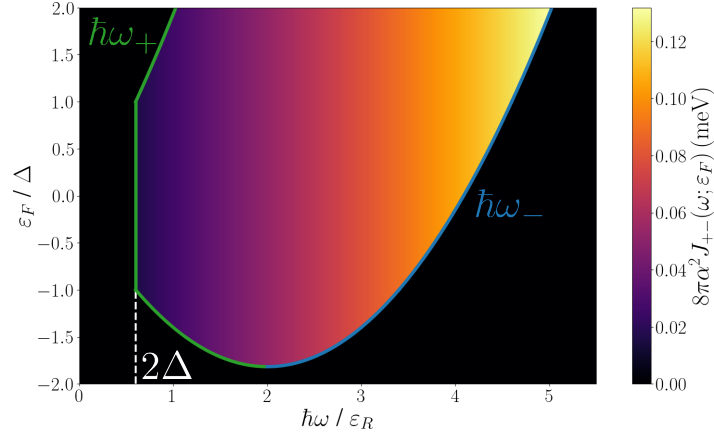


FIG. 5. Joint density of states  $8\pi\alpha^2 J_{+-}(\omega; \varepsilon_F)$  for a gapped 2D anisotropic Rashba model with  $\varepsilon_R > \Delta$ , and the absorption edges  $\hbar\omega_{\pm}(\varepsilon_F)$ . The parameters used are  $\Delta = 0.3\varepsilon_R$ ,  $\alpha = 10\text{ meV\AA}$ , and  $m_x = m_0$ ,  $m_y = 4m_0$  for the effective masses.

which is displayed as a color map in Fig. 5, for a system having  $p < 1$ . For a given value of  $\varepsilon_F$  the color gradation shows the linear dependence on the exciting frequency.

### B. First order spin current conductivity

According to the formula (3), the induced spin current response function of the anisotropic Rashba model becomes

$$\sigma_{ij}^{\ell}(\omega) = -\delta_{\ell z} \frac{e}{8\pi} \frac{1}{2\varepsilon_R} \left[ \varepsilon_{ijz} - i \frac{m_d}{m_i} \left( \frac{2\Delta}{\hbar\tilde{\omega}} \right) \delta_{ij} \right] \left[ A(\tilde{\omega}) + \frac{1}{2} \hbar(\omega_- - \omega_+) \right], \quad (26)$$

where

$$A(x) = \frac{\hbar x}{4} \left[ 1 - \left( \frac{2\Delta}{\hbar x} \right)^2 \right] \ln \left[ \frac{(x + \omega_+)(x - \omega_-)}{(x - \omega_+)(x + \omega_-)} \right]. \quad (27)$$

Remarkably, the linear spin currents generated in this system will have electrons with out-of-plane spin orientations only. This is a consequence of the breaking of TRS by the term  $d_z(\mathbf{k})$ , which is a non null constant in the present model. This makes the product of matrix elements  $\langle \lambda | \hat{\mathcal{J}}_i^{\ell} | -\lambda \rangle \langle -\lambda | \hat{v}_j | \lambda \rangle$  an odd (even) function in  $\mathbf{k}$ -space when  $\ell = x, y$  ( $\ell = z$ ). Thus, the Kubo expression (3) integrates to a non zero value when  $\ell = z$  only. The longitudinal components of the spin current conductivity (Fig. 6(a)) are proportional to the gap parameter,  $\sigma_{ii}^z(\omega) \propto \Delta$ , and therefore they vanish for the gapless case. Moreover, these diagonal components are inversely proportional to  $\sqrt{m_i}$ , such that  $m_x \sigma_{xx}^z(\omega) = m_y \sigma_{yy}^z(\omega)$ , as a consequence of the mass anisotropy. On the other hand, the Hall components are nonzero, regardless of the value of  $\Delta$ , indicating the generation of a spin Hall effect in the gapped or ungapped system. In addition,  $\sigma_{xy}^{\ell}(\omega) = -\sigma_{yx}^{\ell}(\omega)$ , as can be seen in Fig. 6(b). The effect of the position of the Fermi level with respect to the gap, manifests through the critical energies  $\hbar\omega_{\pm}(\varepsilon_F)$ . The variation of Fermi energy leads mainly to a change of the window  $\hbar(\omega_- - \omega_+)$ , just like in JDOS.

If  $\mathbf{E}_0^{\omega} = E_0^{\omega}(\cos \varphi \hat{\mathbf{x}} + \sin \varphi \hat{\mathbf{y}})$  is the amplitude of the external field, the spin current can be written as the sum of a component along  $\mathbf{E}_0^{\omega}$  and a component perpendicular to it,

$$\mathcal{J}^z(\omega) = [\cos^2 \varphi \sigma_{xx}^z(\omega) + \sin^2 \varphi \sigma_{yy}^z(\omega)] \mathbf{E}_0^{\omega} + [\sin \varphi \cos \varphi (\sigma_{xx}^z(\omega) - \sigma_{yy}^z(\omega)) + \sigma_{xy}^z(\omega)] (\mathbf{E}_0^{\omega} \times \hat{\mathbf{z}}), \quad (28)$$

which reduces to  $\mathcal{J}^z(\omega) = \sigma_{xy}^z(\omega) (\mathbf{E}_0^{\omega} \times \hat{\mathbf{z}})$  when  $\Delta = 0$ . Expression (28) suggests how the induced spin current could be manipulated through the frequency dependence of the tensor  $\sigma_{ij}^z$  and the direction of the applied in-plane electric field.

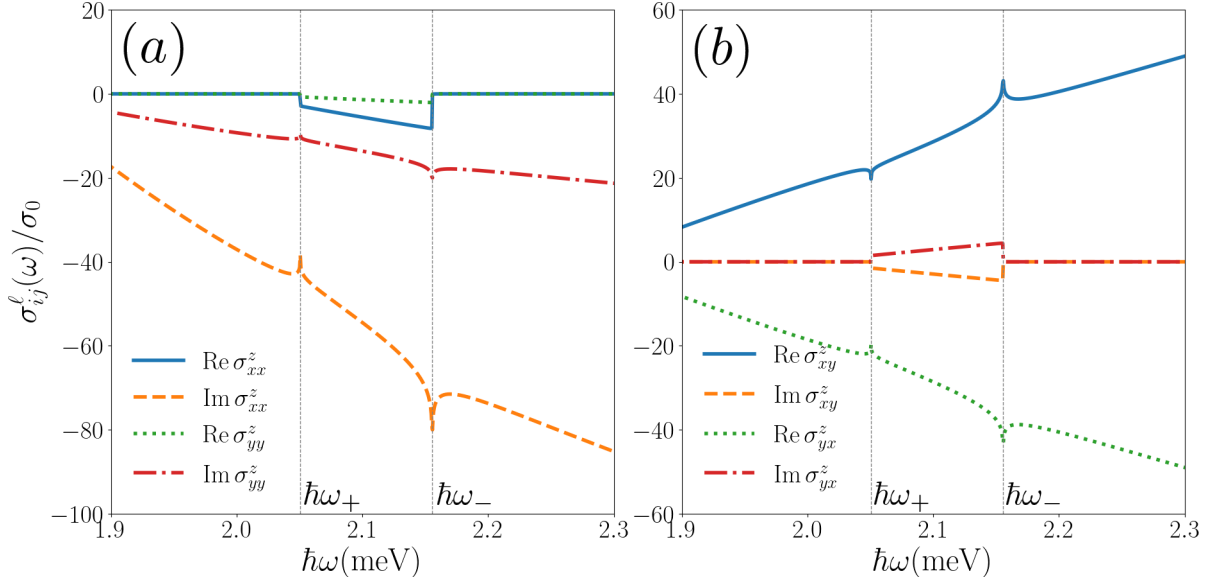


FIG. 6. Longitudinal (a) and Hall (b) components of the linear spin current conductivity tensor  $\sigma_{ij}^z(\omega)$  for a gapped anisotropic Rashba model, normalized to  $\sigma_0 = e/8\pi$ . The parameters used are  $\Delta = 1$  meV,  $m_x = m_0$ ,  $m_y = 4m_0$ ,  $\alpha = 10$  meVÅ,  $\varepsilon_F = 2\Delta$ .

### C. SH spin current conductivity

For the second-harmonic spin current conductivity we obtain the following expressions from (6) (no sum over repeated indices is implied),

$$\sigma_{ijj}^{\ell,(2\omega)}(\omega) = \delta_{\ell j} \varepsilon_{ijz} \frac{e^2/8\pi}{(\hbar\tilde{\omega})^2} \frac{1}{k_R} \left(\frac{m_d}{m_j}\right)^{1/2} F(\tilde{\omega}), \quad (29)$$

$$\sigma_{iii}^{\ell,(2\omega)}(\omega) = \frac{e^2/8\pi}{(\hbar\tilde{\omega})^2} \frac{1}{k_R} \left(\frac{m_d}{m_i}\right)^{3/2} \left\{ \varepsilon_{\ell iz} G(\tilde{\omega}) + 2i(1 - \delta_{\ell z}) \left(\frac{2\Delta}{\hbar\tilde{\omega}}\right) [A(\tilde{\omega}) - A(2\tilde{\omega})] \right\}, \quad (30)$$

$$\sigma_{iji}^{\ell,(2\omega)}(\omega) = \sigma_{iij}^{\ell,(2\omega)}(\omega) = \frac{e^2/16\pi}{(\hbar\tilde{\omega})^2} \frac{1}{k_R} \left(\frac{m_d}{m_i}\right)^{1/2} \left\{ \delta_{\ell i} \varepsilon_{ijz} H(\tilde{\omega}) + 2i(1 - \delta_{\ell z}) \left(\frac{2\Delta}{\hbar\tilde{\omega}}\right) [A(\tilde{\omega}) - A(2\tilde{\omega})] \right\}, \quad (31)$$

where  $k_R = \varepsilon_R/\alpha = m_d\alpha/\hbar^2$ ,  $A(x)$  is given by (27), and

$$F(\tilde{\omega}) = \left\{ 1 + \frac{1}{4} \left[ 1 - \left(\frac{2\Delta}{\hbar\tilde{\omega}}\right)^2 \right] \right\} A(\tilde{\omega}) - \left[ 1 - \left(\frac{2\Delta}{2\hbar\tilde{\omega}}\right)^2 \right] A(2\tilde{\omega}) + \frac{1}{8} \hbar(\omega_- - \omega_+), \quad (32)$$

$$G(\tilde{\omega}) = \left\{ 1 - \frac{3}{4} \left[ 1 - \left(\frac{2\Delta}{\hbar\tilde{\omega}}\right)^2 \right] \right\} A(\tilde{\omega}) - \left\{ 4 - 3 \left[ 1 - \left(\frac{2\Delta}{2\hbar\tilde{\omega}}\right)^2 \right] \right\} A(2\tilde{\omega}) - \frac{3}{8} \hbar(\omega_- - \omega_+), \quad (33)$$

$$H(\tilde{\omega}) = \left\{ 2 - \frac{1}{2} \left[ 1 - \left(\frac{2\Delta}{\hbar\tilde{\omega}}\right)^2 \right] \right\} A(\tilde{\omega}) - 2 \left\{ 2 - \left[ 1 - \left(\frac{2\Delta}{2\hbar\tilde{\omega}}\right)^2 \right] \right\} A(2\tilde{\omega}) - \frac{1}{4} \hbar(\omega_- - \omega_+). \quad (34)$$

A number of conclusions can be derived from these expressions. In contrast to the linear response, the above expressions imply that there is no  $z$ -polarized SH spin current induced in the system,  $\sigma_{ijl}^{z,(2\omega)}(\omega) = 0$ . On the other hand, equation (30) shows that if  $\Delta = 0$  the longitudinal response  $\sigma_{iii}^{\ell,(2\omega)}$  describes a spin current with the spin oriented perpendicularly to the electric field (and to the spin current), while one with parallel spin orientation and current is possible when  $\Delta \neq 0$ . The Hall components  $\sigma_{ijj}^{\ell,(2\omega)}$  (29) generate spin currents with spin always oriented in the direction of the field (normal to the spin current), regardless of the presence of an energy gap. As for the components in (31),  $\sigma_{iij}^{\ell,(2\omega)}(\omega)$  and  $\sigma_{iji}^{\ell,(2\omega)}(\omega)$ , they are associated to a nonlinear current with spin orientation parallel to it when  $\Delta = 0$ , otherwise such an orientation is not fixed for  $\Delta \neq 0$ .

The terms in braces in (29)-(31) involve the masses through the combination  $m_d = \sqrt{m_x m_y}$  only. Thus, the in-plane anisotropy becomes apparent in every non-zero tensor component through a factor of the type  $(m_x/m_y)^{\pm\nu/4}$ ,

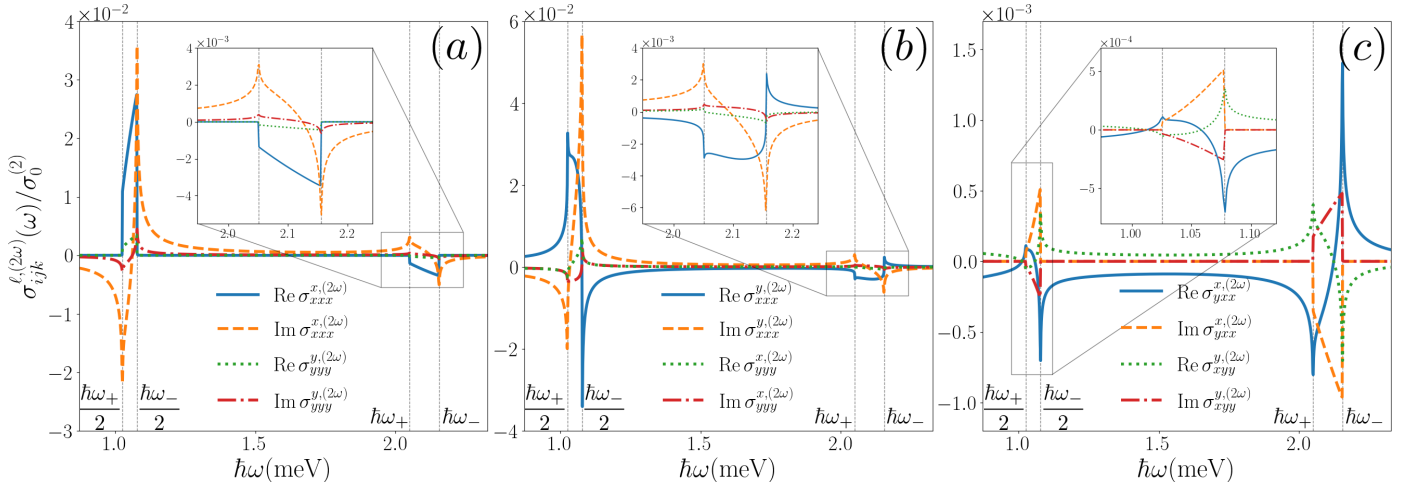


FIG. 7. Second-harmonic spin current conductivity tensor  $\sigma_{ijk}^{\ell,(2\omega)}(\omega)$  for a gapped 2D anisotropic Rashba model, which determines a spin current flowing in direction  $i$ , with the spin polarized along the direction  $\ell$ , induced by the external field components  $j$  and  $l$ . In this system  $\sigma_{ijl}^{z,(2\omega)}(\omega) = 0$ . (a) Longitudinal components with  $i = j = l = \ell$ . (b) Longitudinal components with  $i = j = l \neq \ell$ . (c) Hall components with  $i \neq j = l = \ell$ . The parameters used are the same as in Fig. 6, and  $\sigma_0^{(2)} = e^2/4\pi\varepsilon_R k_R$ .

with  $\nu = 1$  or 3. Figure 7 shows the frequency dependence of the in-plane polarized SH components  $\sigma_{ijl}^{x,(2\omega)}(\omega)$  and  $\sigma_{ijl}^{y,(2\omega)}(\omega)$ . As expected, the spectral structure around  $\hbar\omega_{\pm}$  is now accompanied by new features around the subharmonics  $\hbar\omega_{\pm}/2$ . The overall structure can be modified through Fermi energy variation, given the behavior of the functions  $\hbar\omega_{\pm}(\varepsilon_F)$  observed in Fig. 5.

The SH spin current response (29)-(31) presents characteristic differences with respect to the linear response, as is the case in the model of section III. Diagonal components are present even in absence of an energy gap, subharmonic structure appears in the spectrum, and the spin polarization is no longer out-of-plane, so that a nonlinear spin Hall effect with in-plane spin orientation is generated. These features may be useful in nonlinear optical spintronic devices.

## V. SUMMARY

We calculated the spin conductivity tensors which characterize the electric-dipole induced spin currents at the fundamental and second harmonic frequencies, in two anisotropic systems with SO interaction.

In the case of a 2DEG with R+D[ $hkl$ ], a time-reversal preserving system, the anisotropy arises from the interplay between the Rashba and Dresselhaus couplings, which in turn depends sensitively on the sample growth direction. For a given crystallographic orientation, the spin splitting of the states acquire a particular dependence on the direction in  $\mathbf{k}$ -space. This modify the spectrum of allowed optical transitions, and the JDOS and the spin current responses at  $\omega$  and  $2\omega$  display characteristic spectra. This suggests an additional way to influence the linear and nonlinear spectra by choosing in advance the growth direction of the sample, besides frequency tuning, the modulability of the Rashba strength, or the direction of the applied electric field. We found also that the response functions  $\sigma_{ij}^{\ell}(\omega)$  and  $\sigma_{ijl}^{\ell,(2\omega)}(\omega)$  vanish identically under the SU(2) symmetry conditions found in Ref [35]. There are, however, additional conditions under which specific tensors components vanish, without the requirement of having a collinear SO vector field. Thus, by a proper choice of the growth direction and SO material parameters, one could select the polarization of the linear and SH spin currents according to the direction of flowing.

In the case of the anisotropic Rashba model studied in Sec. IV, the anisotropy is that of a 2D free electron gas with different masses [48],  $m_x \neq m_y$ , in the presence of a Rashba type interaction which introduces different spin splitting along perpendicular directions [41]. To be comprehensive, the model includes an energy gap parameter, which breaks the time-reversal symmetry; when the gap is closed, the model reduces to that studied in Ref. [42]. The band structure offers distinct positions for the Fermi level (above, within, and below the gap), which define several distinguishable scenarios for the allowed optical interband transitions, characterized by the Fermi contours in each case. These manifest in contrasting ways in the linear and SH spin current response. The linear spin conductivity  $\sigma_{ij}^{\ell}(\omega)$  shows that only out-of-plane spin polarized currents develops ( $\ell = z$ ), while the SH spin conductivity tensor

$\sigma_{ijl}^{\ell,(2\omega)}(\omega)$  gives rise to currents with spin orientation lying parallel to the plane of the electron gas ( $\ell = x, y$ ). The longitudinal components  $\sigma_{ii}^{\ell}(\omega)$  are inversely proportional to  $\sqrt{m_i}$ , connected through the masses in the form  $m_x \sigma_{xx}^z(\omega) = m_y \sigma_{yy}^z(\omega)$ , and vanishing for the gapless case. In contrast, the Hall components are non null regardless of the presence of a gap, depend on the masses through the geometric mean  $\sqrt{m_x m_y}$  only, and satisfy  $\sigma_{yx}^{\ell}(\omega) = -\sigma_{xy}^{\ell}(\omega)$ . On the other hand, the SH components are proportional to the ratio of masses in the combination  $(m_x/m_y)^{\pm 1/4}$  or  $(m_x/m_y)^{\pm 3/4}$ .

In summary, we investigated the spectral properties of the linear and nonlinear optical spin conductivities of two anisotropic models for SO coupled systems, and its dependence on a number of physical quantities like the exciting frequency, the position of the Fermi level, energy gap, mass anisotropy, SO strengths, Rashba and Dresselhaus couplings interplay for arbitrary sample growth directions, or the direction of the externally applied electric field, according to each case. The presence of anisotropy introduces optical signatures which in turn may be useful to identify or estimate some of these material parameters. In particular, the models illustrate the existence of the nonlinear spin Hall effect in systems with SO interaction, under the presence or absence of time-reversal symmetry. The results suggest different ways to manipulate the optically induced linear and SH spin current responses, which could find spintronic applications. We hope that this work will stimulate further investigations under more general conditions, such as the presence of extrinsic SO mechanisms or the use of a conserved spin current definition [44, 50].

- 
- [1] K. S. Novoselov, A. K. Geim, S. V. Morozov, D. Jiang, Y. Zhang, S. V. Dubonos, I. V. Grigorieva, and A. A. Firsov, *Science* **306**, 666 (2004).
- [2] S. Bandyopadhyay and M. Cahay, *Introd. to Spintron.* (CRC Press, 2015).
- [3] R. Winkler, *SpinOrbit Coupling Effects in Two-Dimensional Electron and Hole Systems*, Springer Tracts in Modern Physics, Vol. 191 (Springer, Berlin, Heidelberg, 2003).
- [4] Y. K. Kato, R. C. Myers, A. C. Gossard, and D. D. Awschalom, *Science* **306**, 1910 (2004).
- [5] V. Sih, R. C. Myers, Y. K. Kato, W. H. Lau, A. C. Gossard, and D. D. Awschalom, *Nat. Phys.* **1**, 31 (2005).
- [6] J. Schliemann, J. C. Egues, and D. Loss, *Phys. Rev. Lett.* **90**, 4 (2003).
- [7] H. C. Koo, J. H. Kwon, J. Eom, J. Chang, S. H. Han, and M. Johnson, *Science* **325**, 1515 (2009).
- [8] J. D. Koralek, C. P. Weber, J. Orenstein, B. A. Bernevig, S. C. Zhang, S. MacK, and D. D. Awschalom, *Nature* **458**, 610 (2009).
- [9] A. Manchon, H. C. Koo, J. Nitta, S. M. Frolov, and R. A. Duine, *Nat. Mater.* **14**, 871 (2015).
- [10] G. Bihlmayer, P. Noël, D. V. Vyalikh, E. V. Chulkov, and A. Manchon, *Nat. Rev. Phys.* **4**, 642 (2022).
- [11] D. Bercioux and P. Lucignano, *Reports Prog. Phys.* **78**, 106001 (2015).
- [12] J. A. Maytorena, C. López-Bastidas, and F. Mireles, *Phys. Rev. B* **74**, 235313 (2006).
- [13] S. M. Badalyan, A. Matos-Abiague, G. Vignale, and J. Fabian, *Phys. Rev. B* **79**, 205305 (2009).
- [14] B. A. Bernevig, J. Orenstein, and S. C. Zhang, *Phys. Rev. Lett.* **97**, 236601 (2006).
- [15] J. Schliemann, *Rev. Mod. Phys.* **89**, 011001 (2017).
- [16] F. Dettwiler, J. Fu, S. Mack, P. J. Weigele, J. C. Egues, D. D. Awschalom, and D. M. Zumbühl, *Phys. Rev. X* **7**, 031010 (2017).
- [17] N. S. Averkiev, M. M. Glazov, and S. A. Tarasenko, *Solid State Commun.* **133**, 543 (2005).
- [18] J. Schliemann, D. Loss, and R. M. Westervelt, *Phys. Rev. B* **73**, 085323 (2006).
- [19] T. Biswas and T. K. Ghosh, *J. Phys. Condens. Matter* **24**, 185304 (2012).
- [20] Z. Li, F. Marsiglio, and J. P. Carbotte, *Sci. Rep.* **3**, 1 (2013).
- [21] B. M. Norman, C. J. Trowbridge, J. Stephens, A. C. Gossard, D. D. Awschalom, and V. Sih, *Phys. Rev. B* **82**, 081304 (2010).
- [22] E. Y. Sherman and J. E. Sipe, *Phys. Rev. B* **73**, 205335 (2006).
- [23] M. M. Glazov, *Phys. Rev. B* **70**, 1 (2004).
- [24] G. Wang, A. Balocchi, A. V. Poshakinskiy, C. R. Zhu, S. A. Tarasenko, T. Amand, B. L. Liu, and X. Marie, *New J. Phys.* **16**, 045008 (2014).
- [25] V. V. Belykh, V. V. Belykh, M. V. Kochiev, D. N. Sob'Yanin, D. R. Yakovlev, D. R. Yakovlev, M. Bayer, and M. Bayer, *Phys. Rev. B* **101**, 235307 (2020).
- [26] M. Prada and D. Pfannkuche, *Phys. Rev. B* **95**, 045421 (2017).
- [27] A. Krzyżewska and A. Dyrdał, *Phys. E Low-dimensional Syst. Nanostructures* **135**, 114961 (2022).
- [28] A. Manchon and S. Zhang, *Phys. Rev. B* **79**, 094422 (2009).
- [29] P. Gambardella and I. M. Miron, *Philos. Trans. R. Soc. A* **369**, 3175 (2011).
- [30] K. Hamamoto, M. Ezawa, K. W. Kim, T. Morimoto, and N. Nagaosa, *Phys. Rev. B* **95**, 224430 (2017).
- [31] H. Kurebayashi, J. Sinova, D. Fang, A. C. Irvine, T. D. Skinner, J. Wunderlich, V. Novák, R. P. Campion, B. L. Gallagher,

- E. K. Vehstedt, L. P. Zârbo, K. Výborný, A. J. Ferguson, and T. Jungwirth, *Nat. Nanotechnol.* **9**, 211 (2014).
- [32] A. Matos-Abiague and R. L. Rodríguez-Suárez, *Phys. Rev. B* **80**, 094424 (2009).
- [33] M. Studer, M. P. Walser, S. Baer, H. Rusterholz, S. Schön, D. Schuh, W. Wegscheider, K. Ensslin, and G. Salis, *Phys. Rev. B* **82**, 235320 (2010).
- [34] B. Zhou, *Phys. Rev. B* **81**, 075318 (2010).
- [35] M. Kammermeier, P. Wenk, and J. Schliemann, *Phys. Rev. Lett.* **117**, 236801 (2016).
- [36] A. S. Kozulin, A. I. Malyshev, and A. A. Konakov, *J. Phys. Conf. Ser.* **816**, 012023 (2017).
- [37] A. S. Kozulin and A. I. Malyshev, *Phys. Rev. B* **99**, 035305 (2019).
- [38] D. Iizasa, M. Kohda, U. Zülicke, J. Nitta, and M. Kammermeier, *Phys. Rev. B* **101**, 245417 (2020).
- [39] A. Pan and D. C. Marinescu, *Phys. Rev. B* **99**, 245204 (2019).
- [40] S. Ahn and S. Das Sarma, *Phys. Rev. B* **103**, 165303 (2021).
- [41] Z. S. Popović, J. M. Kurdestany, and S. Satpathy, *Phys. Rev. B* **92**, 035135 (2015).
- [42] S. Saberi-Pouya, T. Vazifeshenas, T. Salavati-Fard, M. Farmanbar, and F. M. Peeters, *Phys. Rev. B* **96**, 075411 (2017).
- [43] S. Saberi-Pouya, T. Vazifeshenas, M. Saleh, M. Farmanbar, and T. Salavati-Fard, *J. Appl. Phys.* **123**, 174301 (2018).
- [44] T. W. Chen, J. H. Li, and C. D. Hu, *Phys. Rev. B* **90**, 195202 (2014).
- [45] L. C. Gomes and A. Carvalho, *Phys. Rev. B* **92**, 085406 (2015).
- [46] C. Kamal, A. Chakrabarti, and M. Ezawa, *Phys. Rev. B* **93**, 125428 (2016).
- [47] M. Zeraati, S. M. Vaez Allaei, I. Abdolhosseini Sarsari, M. Pourfath, and D. Donadio, *Phys. Rev. B* **93**, 085424 (2016).
- [48] S. Ahn and S. Das Sarma, *Phys. Rev. B* **103**, L041303 (2021).
- [49] A. Dyrdał, J. Barnaś, and V. K. Dugaev, *Phys. Rev. B* **95**, 245302 (2017).
- [50] J. Shi, P. Zhang, D. Xiao, and Q. Niu, *Phys. Rev. Lett.* **96**, 076604 (2006).